Key Engineering Materials
ISSN: 1662-9795, Vols. 233-236, pp 615-620
doi:10.4028/www.scientific.net/KEM.233-236.615

Online: 2003-01-15

Atomistic Deformation of Silicon under Triaxial Stresses

K. Mylvaganam and L.C. Zhang

School of Aerospace, Mechanical and Mechatronic Engineering, The University of Sydney, Sydney NSW 2006, Australia

Keywords: Atomistic Deformation, Silicon, Tersoff Potential, Triaxial Stress

Abstract. This paper presents the structural transitions of diamond cubic silicon under triaxial tension and compression at the atomistic scale using molecular dynamics analysis. The simulation shows under tension, a small portion of the diamond cubic silicon transforms into trigonal planar silicon before fracture and this is a reversible transformation. Under compression, diamond cubic silicon transforms into β-silicon and then to hexagonal prism. On unloading both of these phases shows plasticity.

Introduction

Single crystalline silicon is a widely used material in micro-electro-mechanical-systems (MEMS). However, during a mechanical process it often experiences external loading that lead to reversible/irreversible phase transformations and fracture. To understand the deformation mechanisms of silicon, many loading cases have been investigated, such as indentation, contact sliding and hydrostatic compression [1-26].

Pressure induced phase transformations of silicon [6-20] have challenged both theorist and experimentalist over the last two decades. So far twelve different structural phases, which are either stable or metastable at different pressure ranges, have been reported. On increasing the pressure, it is well known that the first phase transformation from the diamond cubic structure (Si-I) to the β-tin structure (Si-II) happens around 12 GPa [11, 12] . Next phase transformation to the simple hexagonal silicon (Si-V) was thought to take place at around 16 GPa [11, 12] . Later, the existence of an intermediate orthorhombic phase, with space group *Imma* was identified between 13 and 16 GPa. An undefined phase (Si-VI) was found at 38 GPa [12-14] and recently its space group was determined as *Cmca* having a base-centred orthorhombic cell with eight atoms [15]. Two other high-pressure phases such as hexagonal-closed-packed, (hcp) (Si-VII) at around 42 GPa [14] and face-centred-cubic, (fcc) (Si-X) at around 79 GPa [13, 14] have also been identified. On decreasing the pressure four other metastable phases were known depending on the depressurisation rate. On slow decompression, β-tin phase (Si-II) transforms first to R8 (Si-XII), which exists over a relatively wide pressure range of 2-12 GPa before converting to BC8 (Si-III) [6, 7] . On very fast decompression of Si-II to atmospheric pressure, two other tetragonal phases Si-VIII and Si-IX have been found [16] .

On the other hand, pressure induced theoretical studies [17-20] are very limited. Recently Mujica et al [20] reported a theoretical study of the high-pressure phase diagram using the density functional theory within the local density approximation. They investigated the relative stability of the different phases by calculating their total energy. Yin et al [18] presented a microscopic study of the properties of pressure induced phase transformation employing an *ab initio* pseudo potential method. Uemura [21, 22] had studied the behaviour of diamond under uniaxial compressive and tensile stress by atomistic simulation method and reports the fracture strength of diamond in compression to be (1.8-4.3) x 10^2 GPa and in tension to be 0.8 x 10^2 GPa.

This paper investigates the deformation of silicon under triaxial compressive and tensile stresses during both loading and unloading.

Method

Molecular dynamics technique is widely known and is used in the present application. Silicon mono-crystal with a control volume of 8.68 x 8.68 x 8.68 nm^3, containing 34353 atoms, was used as the sample in the simulation. The atoms on the outer layer of the sample were taken as thermostat atoms to ensure reasonable outward heat conduction. A three-body Tersoff [23, 24] interatomic potential that takes into account the directionality of bonding was used for the Si-Si interactions. This potential has been used extensively in molecular dynamic studies of silicon. The sample was relaxed for 5 Ps and the stresses were applied by uniformly forced displacements of the atoms on the outer layer along X-, Y- and Z-directions. The atoms in the sample were relaxed after every 0.5 Å displacement for a period of 2.5 Ps and the resulting structures were analysed. The normal stresses (σ_{xx} σ_{yy} and σ_{zz}) were calculated by summing forces across the outermost YZ, XZ and XY planes and dividing it by the initial area. The mechanics model is shown in Fig. 1.

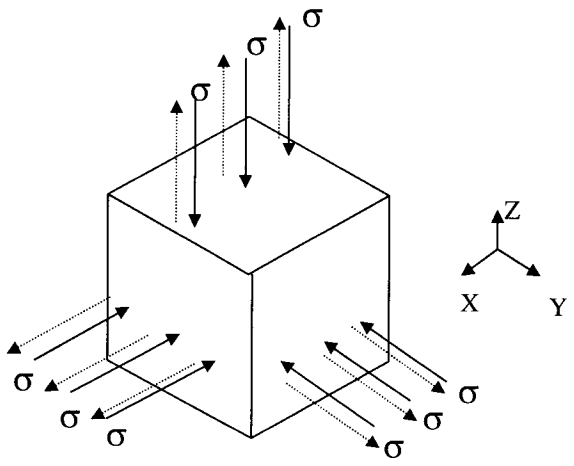

Figure 1: The mechanics model for triaxial compression and tension.

Results and Discussion

Substrate under triaxial tension. The stress-strain relationship under triaxial tension is shown in Figure 2. This shows that beyond a strain of 0.432, corresponding to a stress of 21.7 GPa (i.e., little before the material fails), the stress increases sharply indicating the possibility of a phase transformation and the sample fails when the stress reaches 67.2 GPa. Thus the failure strength of silicon in triaxial tension is 21.7-67.2 GPa. However, it is safer to work with the tensile strength below 21.7 GPa. On releasing the stress from 39.2 GPa, the unloading curve coincides with the loading curve showing that there is no plastic deformation. This shows that the phase transformation is reversible and the material behaves elastically until it fails.

We also did a uniaxial tension test in a similar manner and found the Poisson's ratio is 0.32. From figure 2, when the applied strains are small, the bulk modulus is 68.73 GPa and this gives a Young's modulus of 74.2 GPa. In the literature a series of values ranging from 64 – 166 GPa have been reported.

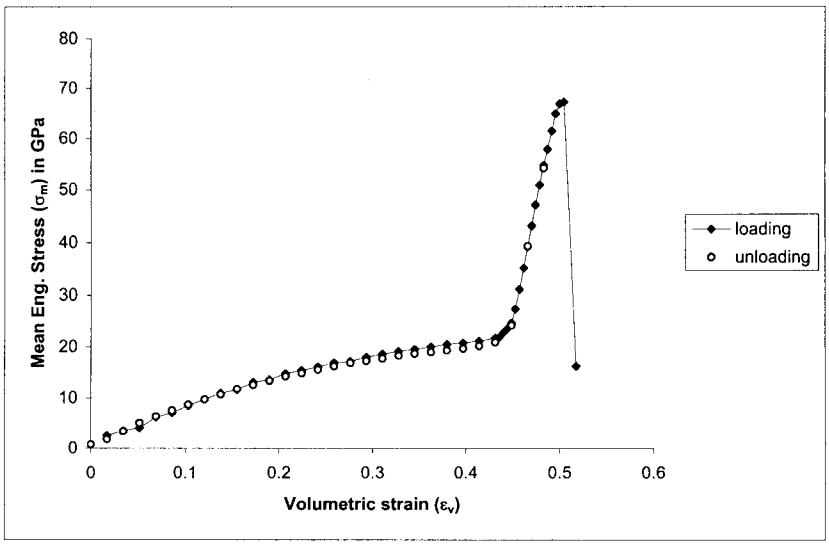

Figure 2: Stress-strain relationship under triaxial tension

An investigation into the coordination number of the atoms reveals that there is an increase in the number of 3-coordinated atoms between 39 GPa and 67 GPa. These 3-coordinated atoms have a trigonal-planar structure with an average bond length of 2.72 Å and they are formed near edges and corners of the sample. A careful study indicates that the 2-coordinated atoms at the boundary initiate this. However, at maximum stress, about 100 atoms transform from the 4-coordinated diamond cubic structure to the 3-coordinated trigonal planar structure. A portion of this new phase having three coordinated atoms obtained in the simulation is shown in Figure 3.

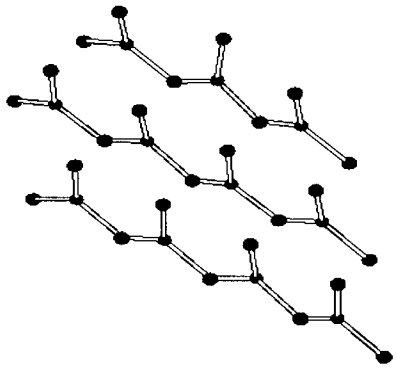

Figure 3: A portion of the trigonal planar phase formed between 39 and 67 GPa.

Substrate under triaxial compression. The stress-strain behaviour under triaxial compression is shown in Figure 4. This shows a non-linear relationship and the stress reaches a maximum at 33.4 GPa. i.e. the simulation model fails at 33.4 GPa. This non-linear stress-strain relationship could be divided into four portions of linear intervals (o-a, a-b, b-c, and c-d), indicating the possibility of three different phase transformations occurring at ~7.36 GPa, ~20.3 GPa, and ~29.2 GPa.

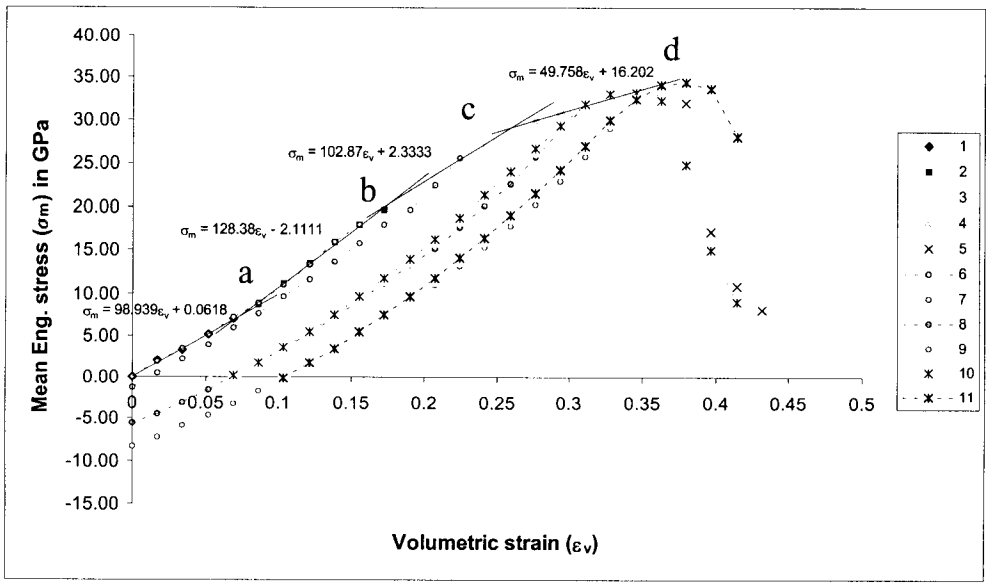

Figure 4: Stress-strain relationship under triaxial compression. (1-5 loading; 6-9 unloading; 10-11 reloading)

An investigation of the nearest neighbours shows that 3-coordinated atoms are formed at ~7.36 GPa. They have trigonal pyramid structure with two equal bonds of 2.22 Å and a third bond of 2.29 Å. These are found mainly at the edges of the sample and a portion of this is shown in Fig. 5. Further investigation shows that these atoms are initially 2-coordinated at the boundary indicating that it could be an artefact due to the boundary effect. On further compression, at about 15 GPa some 5- and 6-coordinated atoms are formed. Significant numbers of 6-coordinated atoms are formed at above 20.3 GPa. A detailed analysis showed that the 6-coordinated atoms formed within 29.0 GPa have a structure closer to β-tin structure and above 29.0 GPa the 6-cordinated atoms corresponds to a new phase having hexagonal prism structure. Actually this is a portion of the hexagonal closest packing arrangement in which six more atoms in the planar hexagonal array are missing. A portion of this new phase obtained is shown in Fig. 6.

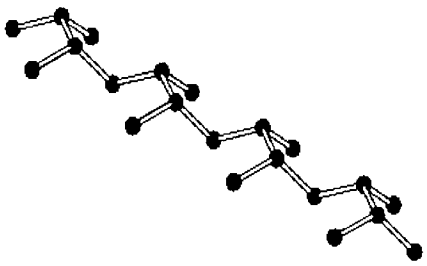

Figure 5: A portion of the trigonal pyramid Phase formed at ~7.36 GPa.

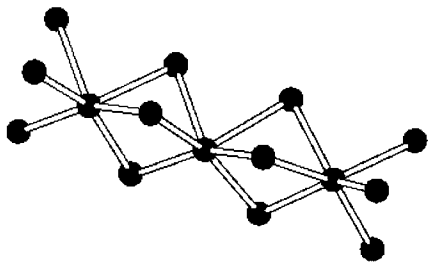

Figure 6: A portion of the hexagonal prism phase formed above 29.0 GPa.

It is interesting to note that according to Hu et al., the transition pressure is lowered by the application of non-hydrostatic stress. For example, for the first phase transformation of diamond cubic silicon to β-tin, Hu et al. reports a value of 11.3-12.5 GPa under hydrostatic conditions compare to a value of ~8.5 GPa under non-hydrostatic conditions. Our molecular dynamics results also show this trend. In this work, the applied stresses are almost hydrostatic (will be hydrostatic when the material is isotropic). We record a value of >15 GPa for diamond to β-tin phase transformation whereas in the molecular dynamics simulation of uniaxial compression and indentation where the stresses are non-hydrostatic, Cheong et al.[25, 26] reported a lower value of ~11 GPa.

However, even at the maximum stress, the total number of transformed atoms is only 11% of the atoms used in the simulation model. Out of this 11% only 3.6% of the atoms are six coordinated and they are mainly found near the sides and the corners of the sample. This indicates that the hydrostatic stress component alone may not be sufficient to bring about complete phase transformation.

On releasing the stress from 17.9 GPa, the unloading curve coincides with the loading curve showing that there is no plastic deformation. However, when the stress was released from 25.6 GPa, the unloading curve followed a slightly different path, showing that there is little plastic deformation. The existence of the 6-coordinated atoms after unloading further confirms the plasticity. A detailed analysis showed the presence of 5-membered rings and atoms with distorted tetrahedral bonding that corresponds to the R8 structure as observed in experiments. The structure showing the presence of a 5-membered ring around 11.6 GPa is shown in Figure 7. On releasing the pressure further, we noticed that the bond formed to give 5-membered ring became little longer. Two other unloading tests starting from 31.7 GPa and 33.4 GPa gave higher amounts of plasticity. All these paths that shows the elastic recovery and the permanent strain that remains on complete unloading are shown in Figure 4 together with the loading curve.

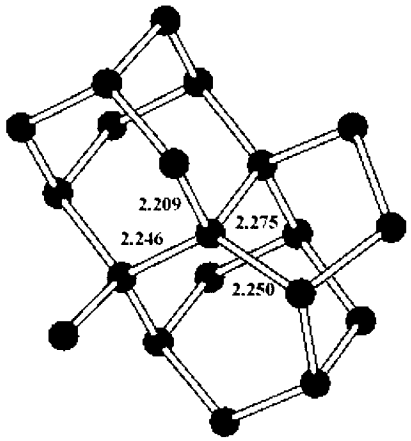

Figure 7: Structure showing the presence of a 5-membered ring and a distorted tetrahedral atom formed around 11.6 GPa during unloading.

On reapplication of the load, the stress-strain curve follows a slightly different path with the stress increases steadily up to a point (yield point) and then the rate of strain-hardening decreases with increasing stress as reported in textbooks. Comparison of the reloading curves show that the rate of strain hardening decreases with the degree of pre-strain. For example, in Figure 4, curve 11

with the higher degree of pre-strain has low rate of strain hardening after the yield point. The reloading curves starting with different permanent strains are shown in Figure 3.

Conclusions

Based on our simulation results we find that the diamond cubic silicon is fully elastic under triaxial tension though a portion of it transforms into another phase at higher pressures; under triaxial compression we have identified two phases β-tin and hexagonal prism before the model fails. Also we find that under hydrostatic stress, the phase transformations take place at higher pressures.

References

[1] V. Domnich, Y. Gogotsi, and S. Dub, Applied Physics Letters **76** (2000), p. 2214.
[2] I. Zarudi and L. C. Zhang, Tribology International **32** (1999), p. 701.
[3] E. R. Weepelmann, J. S. Field, and M. V. Swain, Journal of Materials Science **30** (1995), p. 2455.
[4] L. Zhang and I. Zarudi, Wear **225-229** (1999), p. 669.
[5] L. Zhang and H. Tanaka, Tribology International **31** (1998), p. 425.
[6] R. O. Piltz, J. R. Maclean, S. J. Clark, et al., Physical Review B **52** (1995), p. 4072.
[7] J. Crain, G. J. Ackland, J. R. Maclean, et al., Physical Review B **50** (1994), p. 13043.
[8] K. Mizushima, S. Yip, and E. Kaxiras, Physical Review B **50** (1994), p. 14952.
[9] M. I. McMahon and R. J. Nelmes, Physical Review B **47** (1993), p. 8337.
[10] J. Z. Hu, L. D. Merkle, C. S. Menoni, et al., Physical Review B **34** (1986), p. 4679.
[11] J. Z. Hu and I. L. Spain, Solid State Commun. **51** (1984), p. 263.
[12] H. Olijnyk, S. K. Sikka, and W. B. Holzapfel, Phys. Lett. **103A** (1984), p. 137.
[13] S. J. Duclos, Y. K. Vohra, and A. L. Ruoff, Phys. Rev. Lett. **58** (1987), p. 775.
[14] S. J. Duclos, Y. K. Vohra, and A. L. Ruoff, Physical Review B **41** (1990), p. 12021.
[15] M. Hanfland, U. Schwarz, K. Syassen, et al., Physical Review Letters **82** (1999), p. 1197.
[16] Y. X. Zhao, F. Buechler, J. R. Sites, et al., Solid State Commun. **59** (1986), p. 679.
[17] B. G. Pfrommer, M. Cote, S. G. Louie, et al., Physical Review B **56** (1997), p. 6662.
[18] M. T. Yin and M. L. Cohen, Physical Review B **26** (1982), p. 5668.
[19] R. J. Needs and R. M. Martin, Physical Review B **30** (1984), p. 5390.
[20] A. Mujica, S. Radescu, A. Munoz, et al., Physica Status Solidi B: Basic Research **223** (2001), p. 379.
[21] Y. Uemura, Physical Review B **51** (1995), p. 6704.
[22] Y. Uemura, Physical Review B **49** (1994), p. 6528.
[23] J. Tersoff, Physical Review Letters **56** (1986), p. 632.
[24] J. Tersoff, Physical Review B **39** (1989), p. 5566.
[25] W. C. D. Cheong and L. C. Zhang, Nanotechnology **11** (2000), p. 1.
[26] W. C. D. Cheong and L. C. Zhang, (to be published).